Sweeping piezoelectric patch vibration absorbers

D Casagrande[1], P Gardonio[1] and M Zilletti[2]

[1] Università degli Studi di Udine, DPIA, Via delle Scienze 208, 33100 Udine, Italy
[2] ISVR, University of Southampton, Highfield SO17 1BJ, Southampton, UK

Daniel.Casagrande@uniud.it

Abstract. This paper presents a simulation study concerning the low-mid frequencies control of flexural vibration in a lightly damped thin plate, equipped with five time-varying shunted vibration absorbers. The panel is excited by a rain-on-the-roof broad frequency band stationary disturbance. The absorbers are composed of piezoelectric patches connected to time-varying RL shunt circuits. Continuous, sweeping, variations over time of the shunts are implemented in such a way as to swing the resonance frequency and damping factor of the absorbers within certain ranges and in this way to reduce the resonant response of multiple flexural modes of the hosting plate. A single patch absorber implementing the sweeping shunt is first presented and its performance is compared to that of a classical patch absorber with time-invariant RL shunt. The same analysis is conducted for a multiple patch system using five shunted absorbers. The control performance is assessed considering the spectrum of the total flexural kinetic energy of the system in the 20 Hz to 1000 Hz frequency band. The study shows that the configuration with five time-varying shunted piezoelectric patches reduces the resonance peaks of the kinetic energy spectrum by 5 to 15 dB.

1. Introduction

Forward [1] was one of the first to propose in 1979 the use of shunted piezoelectric transducers to control the vibration of structures. In the following years, several studies were published on this topic [2-9] investigating the basic principles of shunt vibration control and exploring the effects produced by passive and active shunted transducers to enhance the vibration reduction effects. While references [10-13] offer detailed reviews on this subjects, the specific idea of implementing electro-mechanical vibration absorbers using piezoelectric patches connected to RL shunt circuits can be traced to the study carried out by Hagood and von Flotow [5]. Considering the classical work on vibration absorbers [14], they derived the expressions for the resistance and inductance elements of the shunt that would optimise the vibration absorption effect on the resonant response of a specific mode of the structure with the shunted piezoelectric patch. The same effect can be achieved using both series and parallel RL circuits [15]. Moreover, the broad brand vibration absorption can be enhanced by adding a negative capacitance in the shunt, which compensates the inherent capacitance of the piezoelectric transducer to maximise the energy absorption by the shunted transducer [16-19]. In practice this can only be obtained with an appropriate active electrical circuit introducing stability issues. Therefore this study will focus on the use of RL shunts.

The possibility of controlling the flexural response of thin structures over a wide frequency band using time-varying mechanical absorbers composed by classical spring-damper-mass mechanical systems has been explored in recent studies [20,21]. In particular, the implementation of time-varying absorbers has been investigated, whose stiffness and damping parameters are varied within given ranges

to continuously sweep the absorbers fundamental resonance and damping ratio and thus to effectively control the resonant response of the hosting structure within a given frequency band. The practical realization of a sweeping mechanical absorber has also been demonstrated experimentally using a voice coil transducer with the magnet suspended on soft springs [22].

In this work, the effects produced by time-varying shunted piezoelectric patch absorbers bonded on a thin panel are considered. Each electro-mechanical absorber is composed by a piezoelectric patch transducer connected to a RL shunt whose inductive and resistive components are continuously varied in such a way as to set the absorber fundamental resonance and damping ratio to control the flexural response of the panel in the targeted frequency band comprised between 20 Hz and 1 kHz.

The paper is structured in five sections. Section 2 describes the system and introduces the mathematical model along with the state space mathematical formulation used in the numerical calculation of the flexural response of the panel with the time-varying shunted piezoelectric patches. Section 3 contrasts the vibration control effects produced by a time-varying shunted piezoelectric patch and a classical time-invariant shunted piezoelectric patch. Section 4, investigates the vibration control effects produced by an array of five sweeping absorbers each working on a specific sub-band of the targeted frequency range or working asynchronously in the whole targeted frequency range. Finally, Section 5 summarises the principal conclusions of the study.

2. Plate with piezoelectric shunted patches

Figure 1 shows the smart panel considered in this study, which is composed of a thin rectangular aluminium plate with five piezoelectric patches whose physical and geometrical parameters are summarized in table 1 and 2 respectively. As depicted in figure 1(a), the plate is exposed to a white noise rain-on-the-roof excitation, which has been modelled in terms of a 4×4 array of point forces uniformly distributed over the surface of the plate. Figure 1(b) shows the absorbers array with the centre patch bonded on the backside of the plate.

Table 1: *Dimensions and physical parameters of the panel.*

Parameter	Value
dimensions	$l_{xp}\times l_{yp}=414\times314$ mm
thickness	$h_p=1$ mm
density	$\rho_p=2700\,\mathrm{Kg/m^3}$
Young's modulus	$Y_p=7\times10^{10}$ N/m^2
Poisson ratio	$\nu_p=0.33$
Modal damping ratio	$\zeta_p=0.02$

Table 2: *Dimensions and physical parameters of the PZT patches.*

Parameter	Value
dimensions	$a_{pex}\times a_{pey}=80\times80$ mm
thickness	$h_{pe}=0.2$ mm
centre positions $j=2,3,4,5$	$x_{c1}, y_{c1}=l_{xp}/2, l_{yp}/2$ $x_{cj}, y_{cj}=l_{xp}/2\mp60, l_{yp}/2\mp60$
density	$\rho_{pe}=7600$ kg/m^3
Young's modulus	$Y_{pe}^E=5\times10^{10}$ N/m^2
Poisson ratio	$\nu_{pe}^E=0.35$
strain/charge constants	$d_{31}=d_{32}=-150\times10^{-12}$ m/V
permittivity	$\varepsilon_{33}^S=29.2\times10^{-9}$ F/m
capacitance	$C_{pe}=934\times10^{-9}$ F

Table 3: *Single patch systems control range.*

Shunt type	Frequency range
Fixed	39 Hz
Sweeping	30 to 130 Hz

2.1. State space formulation

The electromechanical equations of motion for the response of the plate with the shunted piezoelectric patch time-varying vibration absorber shown in figure 1 are derived with a state-space formulation [23]. This general formulation takes into account a rectangular thin plate with 1 or 5 shunted piezoelectric

absorbers, characterized by time-varying inductance and resistance. The stochastic nature of the primary disturbance acting on the plate and the time-varying characteristics of the shunt circuits of the vibration absorbers cannot be addressed using a standard formulation in the frequency domain for vibrations, based on frequency dependent power spectral densities (PSD) and transfers functions [24]. Thus a state space formulation is used in conjunction with a numerical approach to integrate the equation of motion of this time-variant system.

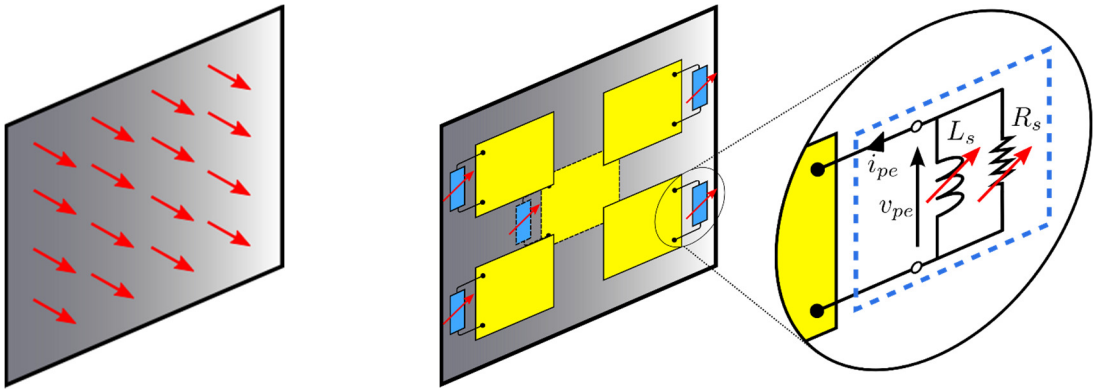

(a) **(b)**

Figure 1. Plate subject to a rain on the roof excitation modelled with a 4×4 array of uncorrelated point forces (a) and equipped with five piezoelectric patches connected to time-varying RL shunts (b).

The formulation considers the classical theory of out of plane flexural vibrations in plates [25], which is based on Kirchhoff hypothesis. Also, the effects of in-plane vibrations are neglected, which is a reasonable assumption in the 20 Hz – 1 kHz frequency range considered in this study. The state space formulation is derived from the generalised form of Hamilton's principle for electromechanical systems [26,27], which, considering displacement and electric field variables, is characterised by the following variational indicator:

$$\text{V.I.} = \int_{t_1}^{t_2} [\delta L + \delta W_{nc}] dt = 0 , \tag{1}$$

where $\delta(\cdots)$ denotes the variation operator and, considering displacement and electric field variables, the Lagrangian is given by [27]:

$$L = T^* - V + W_e^* . \tag{2}$$

Also, T^*, V, W_e^* and W_{nc} are the kinetic coenergy, the elastic potential energy, the electrical coenergy and the work done by non-conservative forces, which are given by the following expressions [3]:

$$T^* = \frac{1}{2}\int_{V_p} \rho_p \dot{w}^2 dV_p + \frac{1}{2}\int_{V_{pe}} \rho_{pe} \dot{w}^2 dV_{pe} , \tag{3}$$

$$V = \frac{1}{2}\int_{V_p} \mathbf{S}_p^t \mathbf{T}_p dV_p + \frac{1}{2}\int_{V_{pe}} \mathbf{S}_{pe}^t \mathbf{T}_{pe} dV_{pe} , \tag{4}$$

$$W_e^* = \frac{1}{2}\int_{A_{pe}} E_{pe} D_{pe} dA_{pe} , \tag{5}$$

$$W_{nc} = -\int_{V_p} \mu \dot{w} w dV_p + \sum_{j=1}^{N} f_{pj} w_j - q_{pe} v_{pe} , \tag{6}$$

In this formulation the superscript "^{t}" indicates matrix transpose and the subscripts "$_p$" and "$_{pe}$" indicate plate and piezoelectric patch variables. Also, $w(x,y,t)$ is the transverse displacement of the plate, $\mathbf{T}_p$, $\mathbf{T}_{pe}$ and $\mathbf{S}_p$, $\mathbf{S}_{pe}$ are 3×1 vectors that contain the T_1, T_2, T_6 and S_1, S_2, S_6 stress and strain components respectively, E_{pe} and D_{pe} are the electric filed intensity and electric displacement. Also μ is the viscous damping factor, f_{pj} are the point forces acting on the plate, and q_{pe}, v_{pe} are the charge and voltage on the piezoelectric patch. Finally V is the volume and A is the surface area. According to Kirchhoff hypothesis, thin plates are characterized by plane strain [28]. However, as discussed by Reddy [29], since the transverse stress component is not considered in the variational formulation, plane stress could be equally assumed, in which case the constitutive equations for the plate and piezoelectric patch are given by the following matrix expressions using the materials axes 1,2,3, which for the problem at hand coincides with the axes x,y,z of the structure [3]:

$$\mathbf{T}_p = \mathbf{c}_p \mathbf{S}_p, \tag{7}$$

$$\begin{bmatrix} D_{pe} \\ \mathbf{T}_{pe} \end{bmatrix} = \begin{bmatrix} \varepsilon_{pe}^S & \mathbf{e}_{pe}^t \\ -\mathbf{e}_{pe} & \mathbf{c}_{pe}^E \end{bmatrix} \begin{bmatrix} E_{pe} \\ \mathbf{S}_{pe} \end{bmatrix}, \tag{8}$$

where

$$\mathbf{c}_p = \begin{bmatrix} \frac{Y_p}{1-\nu_p^2} & \frac{\nu_p Y_p}{1-\nu_p^2} & 0 \\ \frac{\nu_p Y_p}{1-\nu_p^2} & \frac{Y_p}{1-\nu_p^2} & 0 \\ 0 & 0 & \frac{Y_p}{2(1+\nu_p)} \end{bmatrix} \quad \mathbf{c}_{pe}^E = \begin{bmatrix} \frac{Y_{pe}^E}{1-\nu_{pe}^{E\,2}} & \frac{\nu_{pe}^E Y_{pe}^E}{1-\nu_{pe}^{E\,2}} & 0 \\ \frac{\nu_{pe}^E Y_{pe}^E}{1-\nu_{pe}^{E\,2}} & \frac{Y_{pe}^E}{1-\nu_{pe}^{E\,2}} & 0 \\ 0 & 0 & \frac{Y_{pe}^E}{2(1+\nu_{pe}^E)} \end{bmatrix} \tag{9,10}$$

Also, the vector $\mathbf{e}_{pe} = \lfloor e_{31} \quad e_{32} \quad 0 \rfloor^t$ is formed by the e_{31} and e_{32} piezoelectric stress/charge constants and ε_{33}^S is the permittivity of the piezoelectric material. The superscripts "^{S}" and "^{E}" indicate that the parameters have taken assuming constant strain, i.e. $\mathbf{S}_{pe} = 0$, and constant electric field intensity, i.e. $E_{pe} = 0$, respectively. As shown in [3] for example, the ε_{33}^S, e_{31} and e_{32} parameters for the piezoelectric patch are derived from the following equations

$$\varepsilon_{pe}^S = \varepsilon_{pe}^T - \mathbf{d}_{pe}^t \mathbf{c}_{pe}^E \mathbf{d}_{pe}, \mathbf{e}_{pe} = \mathbf{c}_{pe}^E \mathbf{d}_{pe}, \tag{11,12}$$

which refers to the permittivity ε_{pe}^T for constant stress, i.e. $\mathbf{T}_{pe} = 0$, and to the piezoelectric strain/charge constants d_{31} and d_{32} forming the vector $\mathbf{d}_{pe}^t = \lfloor d_{31} \quad d_{32} \quad 0 \rfloor$, which are normally measured and provided in piezoelectric material datasheets. Substitution of equations (3-6) into equation (1) gives the following integral expression

$$\int_{t_1}^{t_2} \Bigg[\int_{V_p} \rho_p \ddot{w} \delta w dV_p + \int_{V_{pe}} \rho_{pe} \ddot{w} \delta w dV_{pe} - \int_{V_p} \delta \mathbf{S}_p^T \mathbf{c}_p \mathbf{S}_p dV_p - \int_{V_{pe}} \delta \mathbf{S}_{pe}^T \mathbf{c}_{pe}^E \mathbf{S}_{pe} dV_{pe} + \int_{V_{pe}} \delta E_{pe} \mathbf{e}_{pe} \mathbf{S}_{pe} dV_{pe} + \int_{V_{pe}} \varepsilon_{pe}^S E_{pe} \delta E_{pe} dV_{pe} - \int_{V_p} \mu \dot{w} \delta w dV_p + \sum_{j=1}^{N} f_{pj} \delta w_j - q_{pe} \delta v_{pe} \Bigg] dt = 0 \tag{13}$$

Considering Kirchhoff hypothesis and assuming small deformations, the linearized strain – displacement relations can be used, which, for the structural axes *x*,*y*,*z* take the following form [25]:

$$\mathbf{S}_p = z\,\mathbf{k}\;\; \mathbf{S}_{pe} = z\,\mathbf{k} \tag{14,15}$$

where $\mathbf{k} = \begin{bmatrix} -w_{,xx} & -w_{,yy} & -2w_{,xy} \end{bmatrix}^{\mathrm{t}}$. Since the piezoelectric material is homogeneous and the piezoelectric patch has constant thickness, the electric field in the piezoelectric patch can be expected to be constant (for small thickness fringe effects are negligible) and thus the following electric field – electric potential relation can be assumed

$$E_{pe} = \frac{v_{pe}}{h_{pe}} \ . \tag{16}$$

Substitution of equations (14-16) into equation (13) leads to the following expression

$$\int_{t_1}^{t_2}\Bigg[-\int_{A_p} m_p \ddot{w}\delta w dA_p - \int_{A_{pe}} m_{pe}\ddot{w}\delta w dA_{pe} - \int_{A_p} I_p \delta\mathbf{k}^T \mathbf{c}_p \mathbf{k} dA_p - \int_{A_{pe}} I_{pe}\delta\mathbf{k}^T \mathbf{c}_{pe}^E \mathbf{k} dA_{pe} + \int_{A_{pe}} z_{pe}\delta v_{pe}\mathbf{e}_{pe}\mathbf{k} dA_{pe} + \int_{A_{pe}} \frac{\varepsilon_{pe}^S}{h_{pe}} v_{pe}\delta v_{pe} dA_{pe} - \int_{A_p} \mu\ddot{w}\delta w dA_p + \sum_{j=1}^{N} f_{pj}\delta w_j - q_{pe}\delta v_{pe} \Bigg] dt = 0 \tag{17}$$

where the volume integrals have been broken into area and thickness integrals, and the thickness integrals have been solved. Here, $z_{pe} = (h_p + h_{pe})/2$, $m_p = \rho_p h_p$, $m_{pe} = \rho_{pe} h_{pe}$, $I_p = h_p^3/12$, $I_{pe} = \alpha h_{pe}^3/12$ with $\alpha = 3(h_p/h_{pe})^2 + 6(h_p/h_{pe}) + 4$. For synchronous motions, the transverse displacement of the plate – piezoelectric patch is separable in space and time variables [23], such that it can be expressed in terms of the following modal summation

$$w(x,y,t) = \begin{bmatrix} \phi_1(x,y) & \cdots & \phi_R(x,y) \end{bmatrix} \begin{bmatrix} q_1(t) \\ \vdots \\ q_R(t) \end{bmatrix} = \boldsymbol{\varphi}(x,y)\mathbf{q}(t) \ , \tag{18}$$

where $\phi_r(x,y)$ are the natural modes of the plate with no piezoelectric patch bonded in it and $q_r(t)$ are the generalized coordinates for the transverse vibrations of the plate. In this study, the plate is assumed simply supported and thus is characterized by the following natural modes and natural frequencies for the *r*-th mode with indices r_1 ,r_2 [30]: $\phi_r(x,y) = 2\sin(k_{xr}x)\sin(k_{yr}x)$ and $\omega_{nr} = \sqrt{\frac{Y_p h_p^2}{12\rho_p(1-\nu_p^2)}}\left(k_x^2 + k_y^2\right)$ with $k_{xr} = r_1\pi/l_x$ and $k_{yr} = r_2\pi/l_y$.

Substituting the modal expansion for the transverse displacement w given in equation (18) and allowing arbitrary variations of $\mathbf{q}(t)$ and $v_{pe}(t)$, such that $\mathbf{q} = 0$ and $v_{pe} = 0$ for $t = t_1, t_2$, leads to the following two matrix equations [3]

$$\left[\mathbf{M}_p + \mathbf{M}_{pe}\right]\ddot{\mathbf{q}}(t) + \mathbf{C}_p\,\dot{\mathbf{q}}(t) + \left[\mathbf{K}_p + \mathbf{K}_{pe}\right]\mathbf{q}(t) - \boldsymbol{\Theta}\,v_{pe} = \boldsymbol{\Phi}_p\,\mathbf{f}_p(t) \, . \tag{19}$$

$$\boldsymbol{\Theta}^t\,\mathbf{q}(t) + C_{pe}\,v_{pe} = q_{pe}(t) \, . \tag{20}$$

Here $C_{pe} = \varepsilon_{pe}^S A_{pe}/h_{pe}$ is the capacitance of the piezoelectric patch and

$$\mathbf{M}_p = m_p \int_{A_p} \boldsymbol{\varphi}^T \boldsymbol{\varphi} dA_p = m_p \mathbf{I} \;\; \mathbf{M}_{pe} = m_{pe} \int_{A_{pe}} \boldsymbol{\varphi}(x,y)^T \boldsymbol{\varphi}(x,y) dA_{pe} \tag{21,22}$$

$$\mathbf{K}_p = I_p \int_{A_p} \boldsymbol{\psi}^T \mathbf{c}_p \boldsymbol{\psi} dA_p = m_p \boldsymbol{\Omega}^2 \;\; \mathbf{K}_{pe} = I_{pe} \int_{A_{pe}} \boldsymbol{\psi}^T \mathbf{c}_{pe}^S \boldsymbol{\psi} dA_{pe} \tag{23,24}$$

$$\mathbf{C}_p = \int_{A_p} \mu \boldsymbol{\varphi}^T \boldsymbol{\varphi} dA_p = 2\xi m_p \boldsymbol{\Omega} \;\; \boldsymbol{\Theta} = z_{pe} \int_{A_{pe}} \boldsymbol{\psi}^T \mathbf{e}_{pe} dA_{pe} \tag{25,26}$$

where $\mathbf{I}$ is a $R \times R$ identity matrix. Also

$$\boldsymbol{\psi} = \begin{bmatrix} \boldsymbol{\varphi}_{,xx} \\ \boldsymbol{\varphi}_{,yy} \\ 2\boldsymbol{\varphi}_{,xy} \end{bmatrix}, \; \boldsymbol{\Omega} = \begin{bmatrix} \omega_{n1} & & \\ & \ddots & \\ & & \omega_{nR} \end{bmatrix}, \; \boldsymbol{\Phi}_p = \begin{bmatrix} \boldsymbol{\varphi}(x_1, y_1) \\ \vdots \\ \boldsymbol{\varphi}(x_{16}, y_{16}) \end{bmatrix}, \; \mathbf{f}_p = \begin{bmatrix} f_{p1} \\ \vdots \\ f_{p16} \end{bmatrix} \tag{27-30}$$

where $f_{p1}, \cdots, f_{p16}$ are the sixteen forces applied on the plate. As schematically shown in figure 1, the piezoelectric patch is connected to a shunt circuit composed by time-varying resistor and inductor components connected in parallel such that

$$i_{pe}(t) = -\frac{1}{R_s} v_{pe}(t) - \frac{1}{L_s} \int v_{pe}(t) dt \,. \tag{31}$$

The electromechanical equation of motion of the shunted piezoelectric patch can now be casted in the following state space matrix formulation

$$\dot{\mathbf{x}}(t) = \mathbf{A}\mathbf{x}(t) + \mathbf{B} f_p(t) \,, \tag{32}$$

$$\dot{\mathbf{q}}(t) = \mathbf{C}\mathbf{x}(t) \,. \tag{33}$$

The state vector is given by

$$\mathbf{x}(t) = \begin{bmatrix} \mathbf{q}(t) \\ \dot{\mathbf{q}}(t) \\ \int v_{pe}(t) \\ v_{pe}(t) \end{bmatrix} \tag{34}$$

and the state, input and output matrices are given by

$$\mathbf{A} = \begin{bmatrix} \mathbf{0} & \mathbf{I} & \mathbf{0} & \mathbf{0} \\ -\mathbf{M}^{-1}\mathbf{K} & -\mathbf{M}^{-1}\mathbf{C}_p & \mathbf{0} & \mathbf{M}^{-1}\boldsymbol{\Theta}_{pe} \\ \mathbf{0} & \mathbf{0} & 0 & 1 \\ \mathbf{0} & -\boldsymbol{\Theta}_{pe}^t / C_{pe} & -1/(C_{pe}L_s) & -1/(C_{pe}R_s) \end{bmatrix}, \quad \mathbf{B} = \begin{bmatrix} \mathbf{0} \\ -\mathbf{M}^{-1}\boldsymbol{\Phi}_p^T \\ \mathbf{0} \\ \mathbf{0} \end{bmatrix}, \quad C = \begin{bmatrix} 0 & \mathbf{I} & 0 & 0 \end{bmatrix} \tag{35-37}$$

where $\mathbf{M} = \mathbf{M}_p + \mathbf{M}_{pe}$, $\mathbf{K} = \mathbf{K}_p + \mathbf{K}_{pe}$ and $\mathbf{I}$ is a 1×16 vector of ones.

The state space equations are integrated using a numerical method as in reference [20] based on a specific Runge-Kutta algorithm [31]. The algorithm uses a fixed integration step, at each time step the **A** matrix is updated with the proper values so that the integration continues at each step using as initial condition the state vector of the previous iteration.

2.2. Energy formulation

The state-space formulation derived in the previous subsection can be efficiently used to predict the time-response of the plate flexural vibration. However, vibration and noise problems subject to stationary random disturbances are normally studied in the frequency domain by considering the spectra of the response and sound radiation. Since the sweeping operation of the absorbers can be categorized as cyclostationary, as discussed in reference [20], a spectral analysis for the flexural response of the plate can be implemented. Therefore to evaluate the control effects produced on the plate by the four absorber configurations considered in this paper, the power spectral density (PSD) of the total plate flexural kinetic energy is derived, which for simplicity, will be referred to as kinetic energy PSD for the remaining part of the paper. As shown in [32], the kinetic energy PSD can be derived with the following expression [33, 34]:

$$S_K(\omega) = \frac{1}{2}\int_{A_p} \rho_p h_p \lim_{T\to\infty} E\left[\frac{1}{T}\dot{w}^*(x,y,\omega)\dot{w}(x,y,\omega)\right] dA_p \ . \tag{38}$$

Here the superscript * indicates the complex conjugate operator, $\dot{w}(x,y,\omega)$ is the finite Fourier transform of $\dot{w}(x,y,t)$, which can also be expressed in terms of a finite modal expansion over the finite Fourier transform of the generalized modal velocities of the panel $\dot{\mathbf{q}}(\omega)$ as follows:

$$\dot{w}(x,y,\omega) = \boldsymbol{\varphi}(x,y)\,\dot{\mathbf{q}}(\omega)\,. \tag{39}$$

Thus, the PSD of the kinetic energy can be written as:

$$S_K(\omega) = \frac{1}{2}\int_S \rho h \lim_{T\to\infty} E\left[\frac{1}{T}\,\dot{\mathbf{q}}^H(\omega)\boldsymbol{\varphi}^T(x,y)\boldsymbol{\varphi}(x,y)\,\dot{\mathbf{q}}(\omega)\right] dS = \frac{1}{2} m_p\, Tr\left[\mathbf{S}_{qq}(\omega)\right], \tag{40}$$

where m_p is the mass of the plate and $Tr\left[\mathbf{S}_{qq}(\omega)\right]$ is the trace matrix of the fully populated matrix $\mathbf{S}_{qq}(\omega)$ containing the self and cross PSD functions of the plate modal velocities produced by the random excitation:

$$\mathbf{S}_{qq}(\omega) = \frac{1}{2}\lim_{T\to\infty} E\left[\frac{1}{T}\ \dot{\mathbf{q}}(\omega)\dot{\mathbf{q}}^H(\omega)\right]. \tag{41}$$

The vector $\dot{\mathbf{q}}(\omega)$ with the finite Fourier transforms of the panel modal velocities can be derived from the combination of the Fourier transforms of equations (19), (20), (31). Since $i_{pe} = dq_{pe}/dt$, and considering that, for the notation shown in figure 1(b), the impedance of the shunt is given by $Z_s = -v_{pe}(\omega)/i_{pe}(\omega)$, the vector $\dot{\mathbf{q}}(\omega)$ can be expressed as follows:

$$\dot{\mathbf{q}}(\omega) = \mathbf{Y}(\omega)\mathbf{f}_p(\omega)\,, \tag{42}$$

where:

$$\mathbf{Y}(\omega) = j\omega\left[-\omega^2\mathbf{M} + j\omega\left(\mathbf{C}_p + Z_{spe}\boldsymbol{\Theta}_{pe}\boldsymbol{\Theta}_{pe}^T\right) + \mathbf{K}\right]^{-1}\boldsymbol{\Phi}_p\,, \tag{43}$$

and $\mathbf{f}_p(\omega)$ contains the finite Fourier transform of the *M* primary forces acting on the panel and $Z_{spe} = (Z_S^{-1} + j\omega C_{pe})^{-1}$. Thus, the matrix $\mathbf{S}_{qq}(\omega)$ with the PSDs of the plate modal velocities can be derived with the following equation:

$$\mathbf{S}_{qq}(\omega) = \frac{1}{2}\lim_{T\to\infty} E\left[\frac{1}{T}\,\mathbf{Y}(\omega)\mathbf{f}_p(\omega)\mathbf{f}_p^T(\omega)\mathbf{Y}^H(\omega)\right] = \frac{1}{2}\mathbf{Y}(\omega)\mathbf{S}_{\mathbf{f}_p\mathbf{f}_p}(\omega)\mathbf{Y}^H(\omega)\,, \tag{44}$$

where $\mathbf{S}_{\mathbf{f}_p\mathbf{f}_p}(\omega)$ is the matrix with the PSD functions of the 16 uncorrelated white noise forces acting on the plate, which, assuming unit primary excitation, is given by a (16×16) identity matrix. In summary, the kinetic energy PSD can be derived by substituting equation (44) into equation (40) so that:

$$S_K(\omega) = \frac{1}{4} m_p Tr\left[\mathbf{Y}(\omega)\mathbf{S}_{\mathbf{f}_p\mathbf{f}_p}(\omega)\mathbf{Y}^H(\omega)\right]. \tag{45}$$

When the sweeping operation mode is implemented, the system becomes time-variant and the time history of the kinetic energy function is not anymore stationary, therefore the PSD kinetic energy cannot be defined [33, 34]. However, for a smooth sweep, the process can be categorized as cycle-stationary and a Fourier transform analysis can be used to estimate the kinetic energy PSD in the frequency domain [35]. In this case, the PSD of the kinetic energy cannot be derived from equation (45) but should be calculated from equations (40) and (41) after the vector $\dot{\mathbf{q}}(\omega)$ has been derived from the numerical finite Fourier transform of the time domain vector $\dot{\mathbf{q}}(t)$, which is calculated numerically using a stochastic integration algorithm as stated above in the end of Section 2.1.

3. Single patch systems

Simulation results for the plate with the top left piezoelectric patch only are presented in this section. Two cases are investigated considering a classical fixed tuning shunt and the proposed sweeping shunt.

3.1. Fixed tuning shunt

For the fixed tuning operation mode, as indicated in table 3, the RL shunt is tuned to control the flexural response at the first resonance frequency of the plate. Considering figure 2(a), the thin solid black line shows the 22 – 176 Hz spectrum of the flexural kinetic energy of the plate without the piezoelectric patch, which is characterized by a series of five peaks (the last two being only 3 Hz apart from each other) due to the resonances of the panel low order natural modes. The thick solid green line shows the spectrum of the flexural kinetic energy of the plate equipped with the shunted piezo (thick solid green line). In this case it can be noted large reduction, of about 15.5 dB, of the controlled mode resonance peak, and some extra reductions, of about 3, 6 and 2.7 dB, of the following four resonance peaks.

3.1. Sweeping shunt

For the sweeping shunt operation mode, the inductance in the RL shunt is harmonically varied such that the shunt natural frequency is swept between the lower and upper limits of the frequency control range with the following harmonic law:

$$\omega_{sh} = \omega_i + (\omega_f - \omega_i)\sin(\omega_s t)^4, \tag{44}$$

where ω_i and ω_f are the initial and final values of the sweep frequency range listed in table 3 and ω_s is the sweeping circular frequency set to 6 Hz. As discussed in reference [36], this sweeping law is obtained by continuously varying the inductance in the shunt with the following law:

$$L_s = \frac{1}{\omega_{sh}^2 C_{pe}}. \tag{45}$$

Also, as discussed in reference [36], the resistance of the shunt is changed in such a way as to maintain a constant damping ratio equal to 30%. The thick solid red line in figure 2(b) shows the effects produced by the sweeping absorber. The amplitudes of the three resonance peaks in the targeted 30 – 130 Hz control band are effectively controlled. More specifically, reductions of about 11.7, 7, 13 dB are observed for the first three resonance peaks, and about 3 dB for the fourth resonance peak, which lies outside the controlled frequency band.

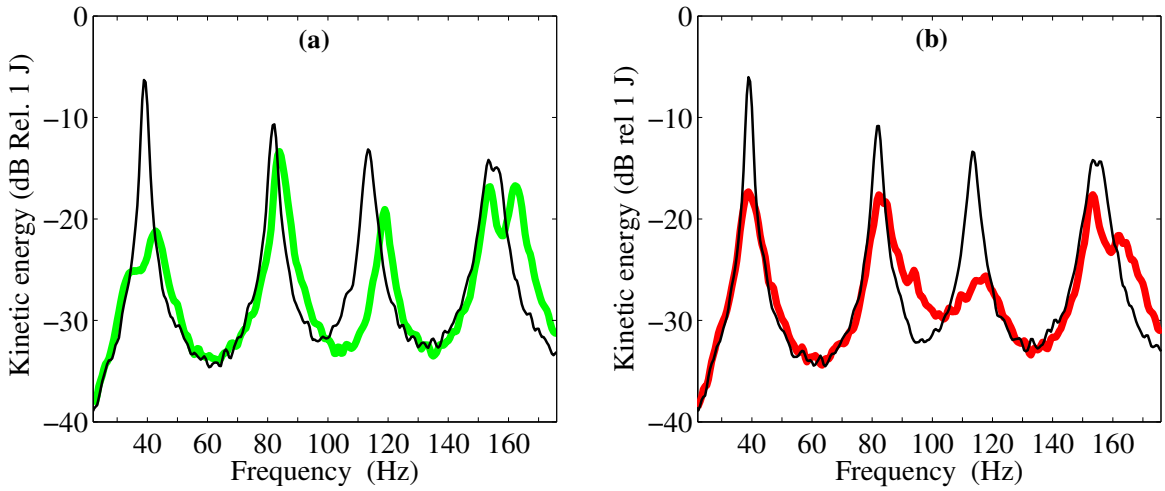

Figure 2. Flexural kinetic energy of the plate with no piezoelectric patch (thin solid black line) and with the top left piezoelectric patch and (a) an RL shunt tuned to the first resonant frequency (thick solid green line);(b) a sweeping shunt tuned to the 30 – 130 Hz frequency band (thick solid red line).

4. Multiple patch systems

The same analysis as that presented in the previous section is introduced here for the panel equipped with five absorbers considering a control frequency range comprised between 22Hz and 1 kHz. Table 4 shows the targeted frequencies for the fixed tuning absorbers. Two operation modes of the sweeping shunted absorbers are considered: first, a series mode in which the control frequency range is divided in five sub-bands and each absorbers is acting on one of them; second, an asynchronous mode in which the five absorbers are acting on the whole control frequency range with a phase shift of $\pi/5$ between each other. In the series operation mode, each one of the five sweeping absorbers is configured to work on one of the five sub-bands, with some overlapping between consecutive bands.

Table 4: *Multi-patch systems control frequencies or control bands.*

Type	Absorber 1	Absorber 2	Absorber 3	Absorber 4	Absorber 5
Fixed	39 Hz	113 Hz	253 Hz	456 Hz	634 Hz
Series sweep	30– 125 Hz	100 – 250 Hz	230 – 440 Hz	400 – 670 Hz	620 –970 Hz
Asynchronous sweep	30 to 970 Hz frequency band with a phase shift of $\pi/5$ between the sweeps				

4.1. Fixed tuning shunts

Figure 3 shows the 22 – 1000 Hz spectrum of the flexural kinetic energy of the plate without the piezoelectric patches (thin solid black line) and with the five piezoelectric patches implementing the fixed tuning shunts (thick solid green line). Each absorber is tuned to control the flexural response at one resonance within each sub-band, which are highlighted by different colours in the plot. At the lower frequencies, the spectrum for the plain plate is characterized by a series of well-defined sharp resonance peaks that start to overlap as frequency rises. The spectrum for the plated with the five fixed tuning absorbers is characterised by smoother peaks. It can be seen that the five fixed absorbers produce respectively reductions of the flexural kinetic energy of around 20 dB, 9 dB, 12 dB and 8 dB at the first four resonances, rather poor control effects between 200 Hz and 300 Hz, and then good reductions of 8 to 15 dB between 300 Hz and 500 Hz and 4 to 10 dB between 550 Hz and 650 Hz.

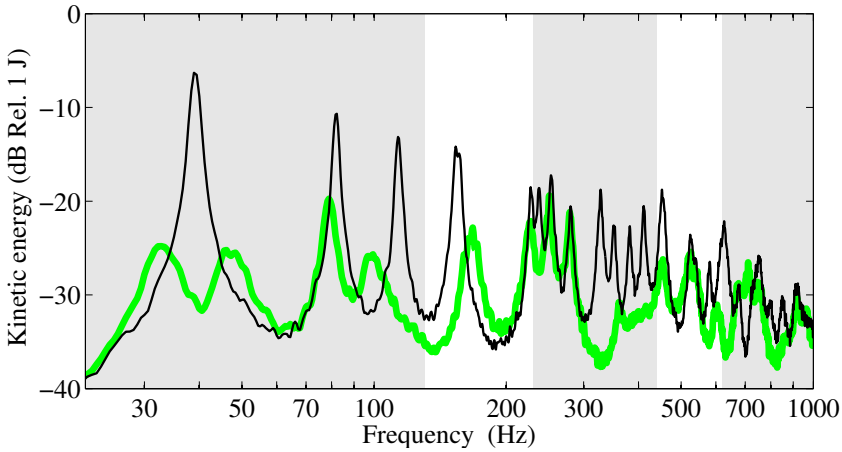

Figure 3. Flexural kinetic energy of the plate with no piezoelectric patch (thin solid black line) and with the five piezoelectric patches implementing RL shunts tuned to the resonance frequencies as specified in table 4 (thick solid green line).

(a)

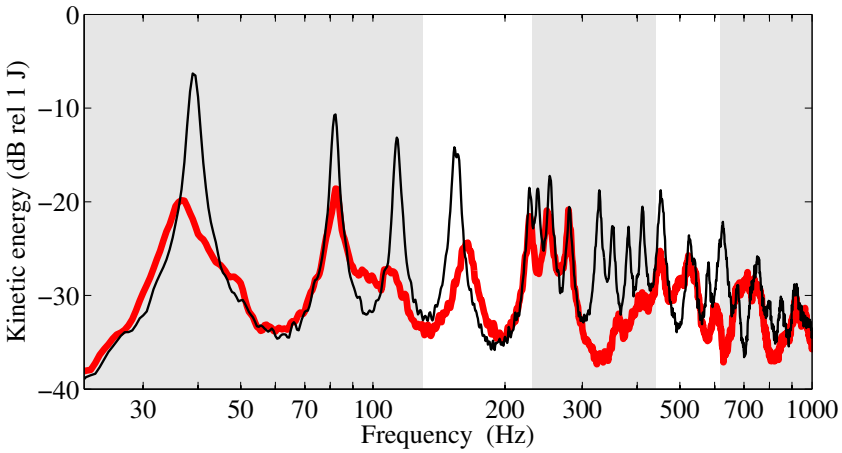

(b)

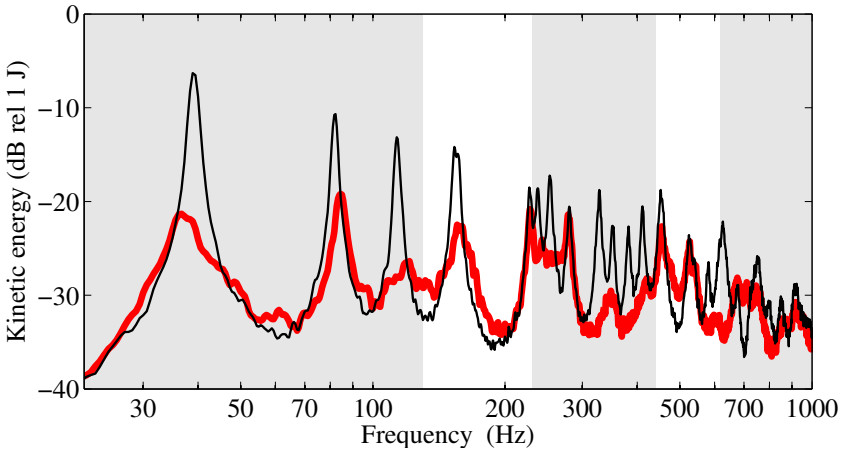

Figure 4. Flexural kinetic energy of the plate with no piezoelectric patch (thin solid black line) and with the five piezoelectric patches (thick solid red line) implementing either the series sweeps (plot a) or asynchronous sweeps (plot b) as specified in table 4.

4.2. Sweeping shunts

The spectrum of the flexural kinetic energy of the plate implementing the series and asynchronous sweeping modes are presented in figure 4 (thick solid red line in plots a,b respectively). In the series mode, the system produces good flexural vibration reductions below 200 Hz, in particular about 14 dB for the first and third resonances and 8 dB for the second one. The performance drops to around 4 dB reduction of the flexural vibration for the resonances comprised in the 200-300 Hz band and then very good control effects are obtained between 300 and 500 Hz, with reductions of the resonance peak amplitudes between 6 and 17 dB. The system also works well between 550 Hz and 650 Hz achieving between 6 and 12 dB and some extra reductions can be seen at higher frequencies in the 750-950 Hz band.

The asynchronous sweeping operation mode also shows very good performances at low and mid frequencies, with improved control effects over the 200-300 Hz band compared to the series mode. However it has lower control effects over the resonances at 450 Hz and 530 Hz. At higher frequencies the control performance is similar to that of the series mode.

5. Conclusions

This simulation study has presented the effects of using time-varying shunted piezoelectric patch absorbers bonded on a thin aluminium panel to control its flexural response in a frequency range comprised between 22 and 1000 Hz. Single and multiple absorbers configuration were analysed, and it could be seen that the proposed system is able to significantly reduce the flexural response of the panel both at low frequencies, where the spectrum of the plate flexural kinetic energy is characterised by well separated resonance peaks, and at mid frequencies, where spectrum of the plate flexural kinetic energy is characterised by wide band crests produced by the overlap of clusters of modes.

Recalling that the sweeping absorbers do not require a precise tuning of the shunts, it is concluded that they can offer significant practical advantages for the development of effective, robust and easy to use modular devices, which can be operated without the need of system identification of the hosting structure physical properties.

Acknowledgements

The authors gratefully acknowledge the European Commission for its support of the Marie Curie program through the ITN EMVeM project (GA 315967).

References

[1] Forward R L 1979 *Applied Optics* **18** (5) 690-697.
[2] Uchino K and Ishii T 1988 *Journal of the Ceramic Society of Japan* **96** (8) 863-867.
[3] Hagood N W Chung W H and von Flotow A 1990 *Journal of Intelligent Material Systems and Structures* **1** (3) 327-354.
[4] Hagood N W and Crawley E F 1991 *Journal of Guidance, Control and Dynamics* **14** (6) 1100-1109.
[5] Hagood N W and von Flotow A 1991 *Journal of Sound and Vibration* **146** (2) 243-268.
[6] Hollkamp J J 1994 *Journal of Intelligent Material Systems and Structures* **5** (1) 49-56.
[7] Johnson C D1995 *Journal of Mechanical Design* **117** (B) 171-176.
[8] Law HH Rossiter PL Simon GP and Koss LL 1996 *Journal of Sound and Vibration* **197** (4) 489-513.
[9] Behrens S Moheimani S O R and Fleming A J 2003 *Journal of Sound and Vibration* **266** (5) 929-942.
[10] Lesieutre G A 1998 Vibration Damping and Control using shunted piezoelectric materials *The shock and Vibration Digest* **30** (3).
[11] Ahmadian Mand DeGuilio P 2001 *The shock and Vibration Digest* **33** (1).
[12] Moheimani S O R 2003 *IEEE Transactions on Control Systems Technology* **11** (1) 482-494.
[13] Moheimani S O R and Fleming A J 2006 *Piezoelectric transducers for vibration control and*

damping (London: Springer-Verlag).
[14] Den Hartog J P 1956 *Mechanical Vibrations* (New York: Reprinted by Dover 1985).
[15] Kozlowski M V Cole D G and Clark R L 2011 *Journal of Vibration and Acoustics* **133** (1).
[16] Tang J and Wang K W 2001 *Smart Materials and Structures* **10** (4) 794-806.
[17] Tsai M S and Wang K W2002 *Smart Materials and Structures* **11** (3) 389-395.
[18] Wu S Y 2001 *Proceedings of SPIE – Smart Structures and Materials 2001: Damping and isolation* Newport Beach CA USA 5-7 March 2001 251-261.
[19] Park C H and Baz A 2005 *Journal of Vibration and Control* **11** 331-346.
[20] Gardonio P and Zilletti M 2013 *Journal of the Acoustical Society of America* **134** (5) 3631-3644.
[21] Gardonio P and Zilletti M 2015 *Journal of Sound and Vibration* **354** 1–12.
[22] Zilletti M and Gardonio P 2015 *Journal of Sound and Vibration* **334** 164–177.
[23] Meirovitch L 1997 *Principles and Techniques of Vibration* (Upper Saddle River, NJ: Prentice Hall).
[24] Newland D E 2005 *An introduction to Random Vibrations, Spectral & Wavelet Analysis* (Mineola, NY: Dover Publications, Inc.).
[25] Reddy J N 2004 *Mechanics of Laminated Composite Plates and Shells: Theory and Analysis* (Boca Raton: CRC Press).
[26] Crandall S H Karnopp D C Kurtz A F and Pridmore-Brown D C 1982 *Dynamics of Mechanical and Electromechanical Systems* (Malabar Fla.: R. E. Krieger Pub. Co.).
[27] Preumont A 2006 *Mechatronics* (Dordrecht: Springer).
[28] Reddy J N 1984 *Energy and Variational Methods in Applied Mechanics* (New York: John Wiley & Sons).
[29] Reddy J N 2006 *Theory and Analysis of Elastic Plates and Shells* (Boca Raton: CRC Press).
[30] Gardonio P and Brennan M JJ 2004 *Mobility and impedance methods in structural dynamics* Ch. 9 in *Advanced applications in acoustics, noise and vibration* Edited by Fahy F and Walker J (London: Spon Press).
[31] Kasdin N J 1995 *J. Guid. Control Dyn.* **18** (1) pp 114-120.
[32] Gardonio P Miani S Blanchini F Casagrande D and Elliott S J 2012 *Journal of sound and vibration* **331** (8) pp 1722-1741.
[33] Bendat J S and Piersol A G 1990 *Random Data Analysis and Measurement Procedures* (Chichester: John Wiley & Sons).
[34] Shin K and Hammond J K 2008 *Foundamentals of signal processing for sound and vibration* (Chichester: John Wiley & Sons).
[35] Gardner W A 1986 *Statistical spectral analysis: a non-probabilistic theory* (Uper Saddle River: Prentice-Hall).
[36] Casagrande D Gardonio P Zilletti 2015 *Proc. 22nd Int. Conf. on Sound and Vibration (Florence)* vol 1 ed Crocker M J Pawelczyk M et al (Red Hook, NY: Curran Associates Inc.) p 747.